Journal of
Computational and Theoretical Nanoscience
Vol. 13, 1–12, 2016

A Complete Road Network Tracking System via Gaussian Hermite Kalman Filter-SLEGION Algorithm on Satellite Images

K. Madhan Kumar[1,*], R. Kanthavel[2], and A. Velayudham[3]

[1] *Faculty of Electronics and Communciation Engineering, PET Engineering College, Vallioor, Tamil Nadu, India*
[2] *Department of ECE, Vellammal Engineering College, Chennai, Tamil Nadu, India*
[3] *Department of Information Technology Cape Institute of Technology, Levengipuram, Tirunelveli District 627114, Tamil Nadu, India*

Road extraction from remotely sensed imagery is highly advantageous for fast road updating in Geographic Information System (GIS) data collection. Several techniques proposed in the literature have met with only partial success on account of complexity of time and accuracy. By reducing the process time and improving the extracted details, we have launched, in this research, an efficient method is proposed to extract road region from the satellite images. Proposed method is made up of three phases: In first phase, the S-LEGION is carried out until stopping criterion is met. Here, an efficient seed point selection technique is performed to the leader selection to S-LEGION. Then, instead of putting an end to the process, the results are passed to the GHKF (Phase II) which tends to recognize the continuation of the road after a likely obstacle or to locate all potential road branches that might exist on the other side of a road junction. Finally, if any road segment cannot be extracted by means of phase I and phase II, faze III goes on with the remaining tracking process by means of S-LEGION. Results are offered for three satellite images. Evaluation for the extracted road networks by means of satellite images shows that the accuracy of our tracker range is to the tune of 98.438% in cluster 10 and 15.

Keywords: S-LEGION, GHKF, leader, Satellite Image, *K*-Means, Pixel.

RESEARCH ARTICLE

1. INTRODUCTION WITH MOTIVATION

Road is one of the important man-made objects whose data is significant in cartography, urban planning, traffic management, and industrial development. Depending on a human operator road extraction methods are classified into automatic and semiautomatic methods.[16] Road extraction from remotely sensed imagery is a quick and economic way to gather transportation data and update a Geographic Information System (GIS) database.[6] Considering that remotely sensed imagery has the potential to characterize urban surfaces,[7] like road and other man-made objects, several methods for extracting road from remotely sensed imagery have been proposed and developed.[8] Generally, semiautomatic strategies function either as road followers, such as approaches proposed by Refs. [10 and 11], or as simultaneous curve-fitting trackers, like approaches based on active contour models,[9] piecewise parabola fitting,[12] and dynamic-programming (DP) optimization.[13] Then again, automated approaches generally require skillful integration of contextual data and a priori knowledge in the road extraction task.[6, 14, 15] Different approaches for the analysis of the tracking the road has been developed in the last two decades.[1–6, 26] Updating the road network information is vital for many applications.

Very high resolution (VHR) optical satellite images with sub metric resolutions furnish novel opportunities for the extraction of information from remote sensing data and the accuracy of the data can be quantitatively improved. Anyhow, details are invisible in lower resolution images but non-road features, can easily disrupt the recognition process, and require more sophisticated modeling for both image and the road network. For the former, the existence of phenomena at multiple scales suggests a multi-scale approach, while for the latter, prior knowledge about the geometry of road network becomes essential.[17] To improve road-extraction accuracy, Dell'Acqua and Gamba[18] employed the fuzzy Hough transform to detect linear features. Song and Civco[19] integrated shape features with pixel wise support vector machine classification outcome to extract road. Shi and Zhu[20] proposed to extract

*Author to whom correspondence should be addressed.

Table I. Summary of related methods in road extraction.

Author	Algorithm type	Application	Limitation	Accuracy	Time
Paolo Gamba et al.[1]	Perceptual grouping algorithm	To enhance urban road network	Accuracy is low	45.48%	N/A
Hu et al.[2]	Toe finding algorithm	To detect the intersection of roads	Road tracker is affected by over extraction	81%	5.35 m
Shao et al.[3]	Fast linear feature detector algorithm	To detect linear features from remote sensing imagery	Difficult to determine the threshold value	N/A	495 ms
He et al.[4]	Multi scale geometric analysis of detector responses	To extract the road feature from the SAR imagery	Poor accuracy due to false detection	74.3%	5 m
Aluir et al.[5]	Dynamic programming algorithm	For extracting the roads in rural areas	Low accuracy	N/A	N/A
Our previous work[24]	UKF and GHKF	Improving accuracy	Needed the performance (time and accuracy)	98.45%	(75–675 sec)
Our method	S-LEGION and GHKF	Decreasing processing time and improving accuracy	N/A	98.48%	(45–350 sec)

road from a binary map by means of the line segment match approach. Although integrating shape features and spectral feature shows a superb performance, it is difficult to obtain a universal linear-feature-extraction method for any situation,[21] and hence further studies are needed. During the road-extraction procedure, once the potential road segments are gathered, a thinning algorithm is usually performed to extract road centerlines.[19] However, the centerlines obtained from thinning algorithms contain many spurs which decrease the smoothness of the centerline. Hence, Smooth-road-centerline extraction should be further studied.

Lots of researches have been conducted for the extraction of satellite images. Some of the recent related works regarding the extraction of satellite images are reviewed in the Table I. A novel method has been implemented by Paolo Gamba et al.[1] for detecting the urban road networks from high-resolution optical/synthetic aperture radar (SAR) images. Perceptual grouping algorithm is employed to recover the local errors and also to reconstruct the regular roads in the images. The main limitation of this method is that it suffers from poor accuracy i.e., the overall accuracy range is only 45.48%. An automatic method for extracting road from aerial imagery is presented by Hu et al.[2] The road extraction task is decomposed into two stages

(i) rectangular approximation to road footprints
(ii) classifying the road footprints through toe finding algorithm.

Due to the over extraction the tracking of road footprints gets affected.

To overcome this defect, a technique is presented by Shao et al.[3] for developing a fast and effective algorithm for detecting ridge- or ribbon-like linear features from remote sensing imagery. Aerial images are employed to test the algorithm's ability to extract roads. A road network grouping algorithm has been developed by He et al.[4] for Synthetic Aperture Radar (SAR) images by utilizing multiscale geometric analysis of detector responses. It functions in three steps.

(1) Extraction of guidance segments
(2) Segment labeling
(3) Grouping the road guidance segments.

A well organized semiautomatic method for 3-D road extraction in rural areas using stereoscopic aerial images is developed by Aluir et al.[5] Experimental results show that the proposed method is efficient and usually yields accurate road centerlines. A new method is implemented by Miao et al.[6] to extract the road centerline from high-resolution imagery based on shape features and multivariate adaptive regression splines (MARS). The main restriction of the proposed method is that the thresholds in the method have to be determined manually and the technique is not relevant for low-resolution images.

By considering the above issues and to improve the road extraction constraints, an efficient approach is urgently needed. In this paper, we have proposed a road extraction approach to recognize the road region from the satellite images. The results of this approach are used to blend the two efficient algorithms for automatic road extraction and time reducing. To prove this point, three totally different phases are developed. Then, performance of the procedure is tested on three diverse satellite images.

The rest of the paper is organized as follows: Introduction with motivation of proposed technique is presented in Section 1. Contribution is discussed in Section 2. The proposed road extraction system is detailed in Section 3. The experimental results and performance evaluation discussion are provided in Section 4. Finally, the conclusions are summed up in Section 5.

2. CONTRIBUTION OF THE PROPOSED APPROACH

Our main contributions are as follows:

- K-means and Euclidean distance are employed to initial leader selection method in S-LEGION process for time consuming and improving the accuracy.

• The proposed road tracking system is more adaptive to roads with high curvature and sharp turns. Now, we present a method to detect the road intersections.

3. PROPOSED AUTOMATIC EXTRACTION OF ROAD NETWORK THROUGH S-LEGION AND GHKF

Updating road network database is vital to several geographic information systems (GIS) application systems like navigation, urban planning, etc. Rapidly changing urban environments accelerate the necessity for frequent updates or revisions of road network databases. With the advent of high-resolution satellite images, there has been a resurgence of research interest in road extraction techniques. Anyhow, due to the extreme complexity of an urban scene, automatic road network extraction continues to be a challenging research topic. Several works are offered in the literature for the extraction of road region from remotely sensed imagery. In this paper, a new approach for road extraction is presented, which is summarized in Figure 1. In our earlier approach,[24] we have developed a road map extraction system with Unscented Kalman Filter and Gauss-Hermite Kalman Filter by means of satellite images. In this paper, an approach is introduced to extend the previous work[24] based on the following two reasons:

• The existing work does not tackle the nonlinearity in segmentation of roads very effectively even though they are non-linear filter prediction.

• The presence of noise in roads affects the performance of forecasting the road pixel when we employ UKF filter. So, we are in need of another non-linear technique in place of UKF filter to the better prediction of road pixels.

In our innovative approach, at the first stage, an S-LEGION based automatic road extraction model is developed to track the road until a stopping criterion is met. Then in the second stage, instead of terminating the process, the results are passed to the Gaussian Hermite Kalman Filter (GHKF) algorithm which tends to find the continuation of the road after a possible obstacle or to locate all possible road branches that might exist on the other side of a road junction. The overall proposed approach is depicted in Figure 1.

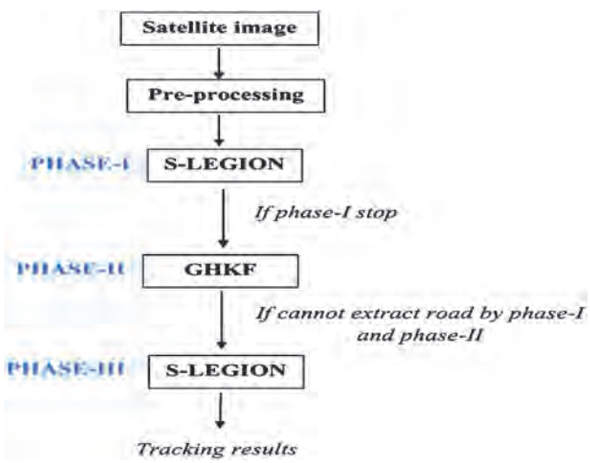

Fig. 1. Overall diagram of proposed road extraction approach.

3.1. Pre-Processing

Initially the input satellite images are preprocessed to eliminate the noises present in the images and to make the images suitable for further processing. In our proposed method pre-processing is carried out through (i) Contrast adjustment (ii) morphological operation (iii) Laplace filter.

(i) Contrast adjustment: The contrast adjustment is mainly performed to smoothen the input images and also to improve the accuracy of road extraction. The contrast adjustment contains several steps like (i) RGB to HSV conversion (ii) V layer-Contrast adjustment (iii) conversion of HSV to RGB (iv) Edge enhancement.

RGB to HSV conversion: In our proposed method the input image used is a color image. For contrast adjustment initially the input satellite image is transformed into HSV image. HSV is the hue, saturation, value color space, in which the hue lies in the range of 0 to 359. The HSV conversion is done by means of the formulae.

For hue

$$H = \text{arc}\frac{(1/2)(2\text{R}-\text{G}-\text{B})}{\sqrt{(\text{R}-\text{G})^2-(\text{R}-\text{B})(\text{G}-\text{B})}} \quad (1)$$

For saturation

$$S_{HSV} = \frac{\max(\text{R},\text{G},\text{B})-\min(\text{R},\text{G},\text{B})}{\max(\text{R},\text{G},\text{B})} \quad (2)$$

For value

$$V_{HSV} = \max(\text{R},\text{G},\text{B}) \quad (3)$$

Where, R is the red component, G is the green component, B is the blue component.

V layer contrast adjustment: After transforming the input satellite image into HSV, contrast adjustment is made in the V layer of the resultant image. The contrast adjustment is done by replacing the pixel below the specified value by black and the pixel above the particular value by white. The pixel which lies in the middle of the two values exhibits grey shades.

Conversion of HSV to RGB: After adjusting the contrast of V layer, the Hue Saturation Value image is converted back to RGB image.

(ii) Smoothen the image using imopen: After contrast adjustment, the morphological operation is performed to eradicate small regions present in the input image. For removing the defects present in the image, morphological opening operation is executed in the image.

Opening: In the opening operation the intensity of the bright region in the image is gradually reduced. It involves both erosion and the dilation operation. The opening operation is performed in two steps.

RESEARCH ARTICLE

1. First the erosion of the image is taken
2. Then the result obtained by erosion undergoes dilation.

$$I_{\text{bin}} \cdot f = (I_{\text{bin}} \oplus f)\Theta f \tag{4}$$

Where, I_{bin} is the binary image. f is the structural element.

(iii) *Laplace filters*: The resultant image obtained from the morphological operation is transmitted through the Laplace filter. The Laplace detects the edge pixels in input satellite image. This helps to enhance the edge in the satellite image.

3.2. Initial Leader Selection

A seed point is the starting point for road extraction process and its selection is very significant to the road tracking results. Many existing methods commence with the selection of seed point furnished by the user. In this approach, we have developed an automatic seed point selection method to extract the road from the satellite image. At first, a reference road model (M_1) with size of 11×11 is manually generated to facilitate initial leader point selection as shown in Figure 4. Then, an initial leader point is generated by matching the reference model with each of the pixel in the satellite image. The procedure of the leader point selection is detailed below:

1. Create the grid structure of the input satellite image.
2. Each grid pixel values are arranged into row format based on the grid structure.
3. Applying k-means algorithm[22] utilized in road extraction in satellite image for the selection of the initial point of the road which has traced path then the minimum distance is calculated based on the following objective function.

$$J = \sum_{i=1}^{k} \sum_{j=1}^{n} \left\| x_j^{(i)} - c_i \right\|^2 \tag{5}$$

Where, $\|x_j^{(i)} - c_i\|^2$ is a chosen distance measure between a data point $x_j^{(i)}$. c_j is the cluster center.

4. For k-means clustering process, firstly k initial (in this technique $k = 10$, 15, and 20) are randomly generated within satellite image.
5. K-clusters are generated by linking every observation with the nearest mean.
6. The centroid of each of the k-clusters becomes the new mean.
7. Steps 5 and 6 are repeated until convergence is reached.
8. The reference model-1 is matched with each cluster; one less distance segment or cluster is obtained using Euclidean distance.

$$Ed_1 = \sum_{R_i, G_i B_i = 1}^{N} \sqrt{\frac{(R_i^1 - R_{ci}) + (G_i^1 - G_{ci}) + (B_i^1 - B_{ci})}{3}} \tag{6}$$

Where, $R_i^1 \rightarrow$ indicates ith pixel point of reference model-1 (for R component), $R_{ci} \rightarrow$ indicates ith pixel point of cth cluster, $G_i^1 \rightarrow$ indicates ith pixel point of reference model-1 (for G component), $G_{ci} \rightarrow$ indicates ith pixel point of cth cluster, $B_i^1 \rightarrow$ indicates ith pixel point of reference model-1 (for B component), $B_{ci} \rightarrow$ indicates ith pixel point of cth cluster.

9. Again, this less distance cluster's pixels is matched with reference model-1; finally, we obtain one less distance cell or pixel using Euclidean distance. From this pixel, we begin the road tracing procedure.

$$Ed_2 = \sum_{R_i, G_i B_i = 1}^{N} \sqrt{\frac{(R_i^1 - RM_{ci}) + (G_i^1 - GM_{ci}) + (B_i^1 - BM_{ci})}{3}} \tag{7}$$

Where, $R_i^1 \rightarrow$ indicates ith pixel point of reference model-1 (for R component), $RM_{ci} \rightarrow$ indicates ith pixel point of cth minimized distance cluster, $G_i^1 \rightarrow$ indicates ith pixel point of reference model-1 (for G component), $GM_{ci} \rightarrow$ indicates ith pixel point of cth minimized distance cluster, $B_i^1 \rightarrow$ indicates ith pixel point of reference model-1 (for B component), $BM_{ci} \rightarrow$ indicates ith pixel point of cth minimized distance cluster.

10. Finally, a reference model-2 (M_2) with size of (11×11) is generated based on the initial seed point as shown in Figure 4. From the center point of reference model-2 (M_2), we can start the road extraction process.

Figure 1 illustrates the general structure and representation of colour image. Each colour images consists of three components: R, G and B. Figure 2 shows reference model-1 which is manually generated based on the road region.

3.3. Phase I: S-LEGION

In this step, our proposed S-LEGION method develops a structure to extract the road network from the satellite image. Normally, Locally Excitatory Globally Inhibitory

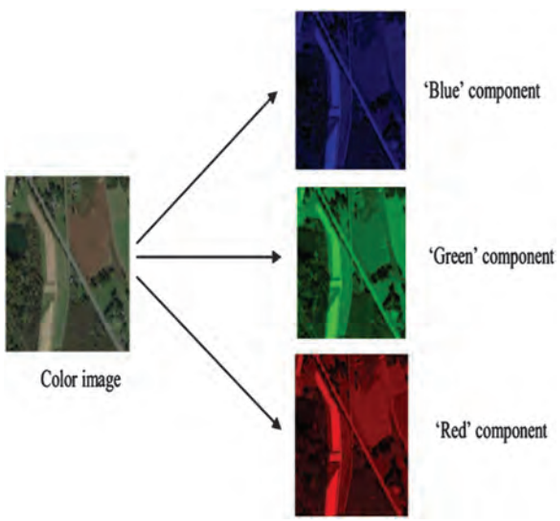

Fig. 2. Colour image and its representation.

RESEARCH ARTICLE

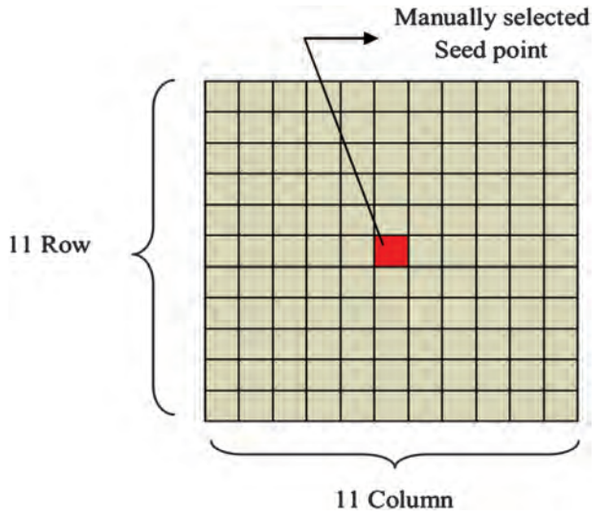

Fig. 3. Reference model-1 (M_1).

Oscillator Networks (LEGION) is based on the concept of oscillatory correlation, where the phases of the neural oscillators encode the binding of the features. The main advantage of LEGION method is that it carries both synchronization and desynchronization of local oscillators. Synchronization is done to extract the road points from the satellite image and desynchronization is mainly performed to group the extracted road points. In LEGION based segmentation method, the initial seed points are generated based on following thresholding conditions. If a total sum $\sum_{k\in N(i)} W_{ik}$ of the coupling weights of all the cells adjacent to cell of interest is larger than a predefined threshold value $\phi_p(\sum_{k\in N(i)} W_{ik} > \phi_p)$, the process sets the variable p_i that indicates whether self-excitation is permitted or not permitted to $p_i = 1$, to determine the cell interest to be self-excitable leader cell. If it is not larger than that $(\sum_{k\in N(i)} W_{ik} \leq \phi_p)$, the process initializes the variable in $p_i = 0$ (self-excitable). The leader cell becomes a candidate of a starting point for the image segmentation process. During this process, any cell or pixel in the whole image can be chosen as leader and we are unable to decide whether the leader is in road region or not. So, initial leader selection is an important step in the LEGION process. To improve the LEGION process, in this section we have proposed a novel method, called S-LEGION, an automatic seed point selection with LEGION based road extraction method from the satellite image. The seed point selection is explained Section 3.2. This method contains two phases namely the silent phase and the active phase; the medial points oscillate between the silent and active phases during the process. The proposed S-LEGION based road extraction of satellite images involves the following stages:

- *Stage* 1: Initialization
- *Stage* 2: Self excitable cell detection
- *Stage* 3: Self excitation
- *Stage* 4: Excitable cell detection
- *Stage* 5: Excitation of dependent cell
- *Stage* 6: Inhibition

According to this algorithm, each cell which corresponds to each pixel enters the non-excitation state, the self-excitable state, and the excitation state and operates in parallel with each other based on the coupling weights between the adjacent eight pixels.

From the above Figure 5, a variable x_i represents whether the cell i is in the excitation state or the non-excitation state. $x_i = 1$ indicates the excitation state and $x_i = 0$ indicates the non-excitation state. Further a variable p_i represents whether the relevant cell is self-excitable or

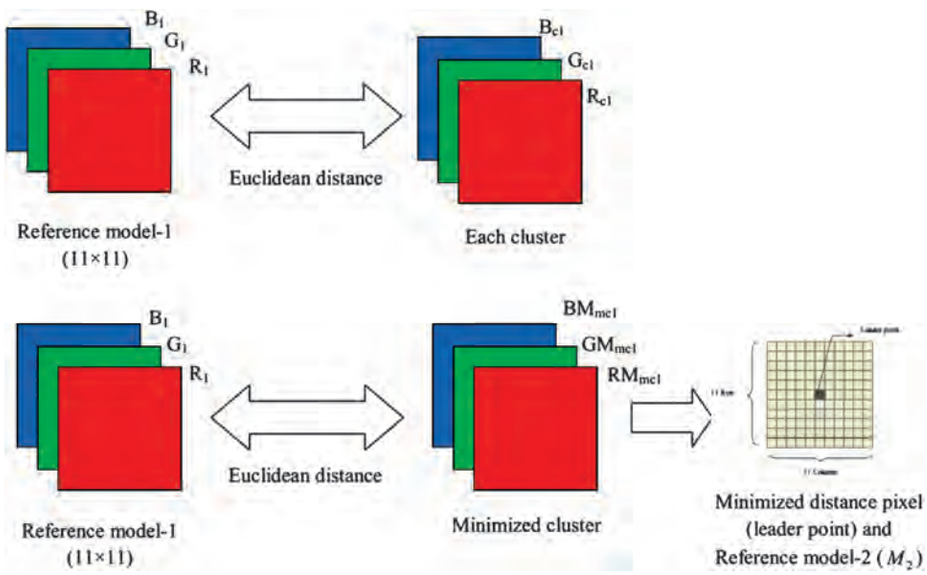

Fig. 4. Seed point selection process.

RESEARCH ARTICLE

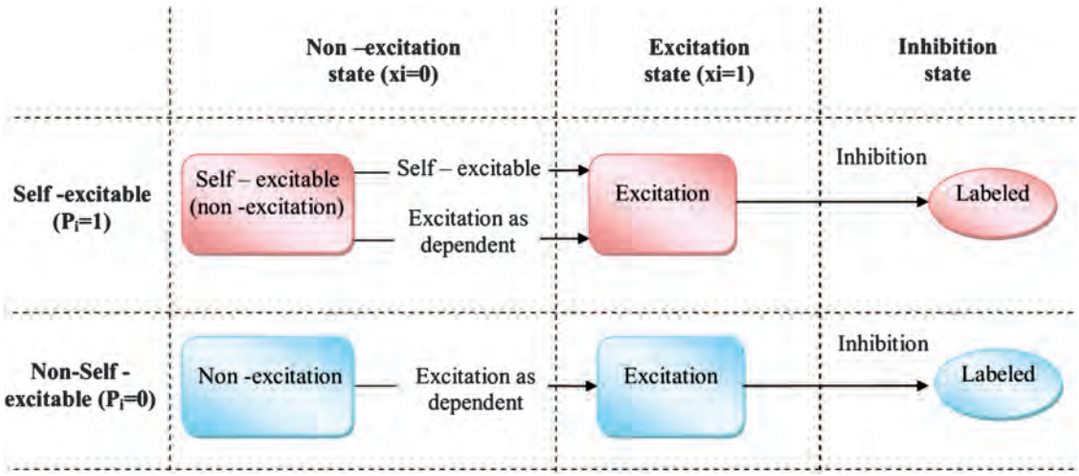

Fig. 5. Cell state transition.

not. $p_i = 1$ indicates that the cell is leader cell and so becomes a self-excitable cell candidate.

Stage 1: *Initialization* ($Z = 0$). In the initial stage of S-LEGION process the global inhibitor is set to zero i.e., $Z = 0$ and all the pixels i are initially placed in the silent phase. Also, at the initialization stage, the process initializes the variable X_i that indicates whether the cell i is in the excitation or non-excitation state, into $X_i = 0$ (non-excitation). The process calculates the coupling weights W_{ik} based on the pixel values of the cells $k \in N(i)$ which are adjacent to the cell (pixel) i.

Where, $N(i)$—represents a set of the cells adjacent to the cell i (for example, a set of the adjacent eight cells). In the case of segmenting a color image, color information can be employed to improve the accuracy of image segmentation. Since the algorithm of the present embodiment makes transition over the cell states by the coupling weights between the adjacent cells (pixels), for example, coupling weights $W(R)_{ik}$, $W(G)_{ik}$ and $W(B)_{ik}$ for the respective red (R), green (G), and blue (B) colors are calculated by following equations:

$$W(R)_{ik} = \frac{I(R)_{\max}}{(1 + |I(R)_i - I(R)_k|)} \tag{8}$$

$$W(G)_{ik} = \frac{I(G)_{\max}}{(1 + |I(G)_i - I(G)_k|)} \tag{9}$$

$$W(B)_{ik} = \frac{I(B)_{\max}}{(1 + |I(B)_i - I(B)_k|)} \tag{10}$$

By calculating an Eq. (11) based on a calculation result of the Eqs. (8)–(10), the inter-cell coupling weight W_{ik} is determined. It is thus possible to realize more accurate image segmentation.

$$W_{ik} = \min\{W(R)_{ik}, W(G)_{ik}, W(B)_{ik}\} \tag{11}$$

Stage 2: *Self excitable cell detection* ($p_i = 1, z_i = 0$). At this stage, the process selects one leader cell (self-excitable candidate) yet to be excited. Here, in proposed S-LEGION process, anyone of the cell or pixel generated by the seed point selection is considered as the leader. The description of the seed point selection is explained in Section 3.2. Now, we consider initial leader as self excitable cell $p_i = 1$.

Stage 3: *Self excitation* ($Z_i = 1, p_i = 1$). In this self excitation stage the leader selected from the self excitable cell detection step is transferred to the active phase. For the selected leader cell the global inhibitor variable is set to 1 i.e., $Z_i = 1$. Once the cell is transferred to the active phase the segmentation begins in that region.

Stage 4: *Excitable cell detection*. After the self excitation stage, the excitable cell detection process is performed. At excitable cell detection, the process verifies the excitation state of the cells $k \in N(i)$ adjacent to the non-excited cell i, and calculates a total sum S_i of the coupling weights of the cells in the excitation state. The total sum S_i is calculated using following formula:

$$S_i = \frac{\sum_{k \in N(i)} W_{ik} * \text{difference}}{\sum_{k \in N(i)} \text{difference}} \tag{12}$$

If the cells $k \in N(i)$ are in the excitation state, that is, $x_k = 1$, the process adds a coupling weight between the cell of interest and the adjacent excited cell $k = S_i$. If this total sum S_i of the coupling weights is larger than the predefined threshold value $\phi_z(S_i > \phi_z)$, the cell i becomes an excitable cell.

Stage 5: *Excitation of dependent cell*. In this stage, the process sets all the excitable cells i detected at "excitable detection" of stage 4 into the excitation state $x_i = 1$ and, simultaneously, $z_i = 1$. Further, the process sets the state variable $z_i = 0$ (no state change) for the cells i which are already into the excitation state ($x_i = 1$ and $z_i = 1$) other than those cells that have been excited at the processing of "excitation of dependent."

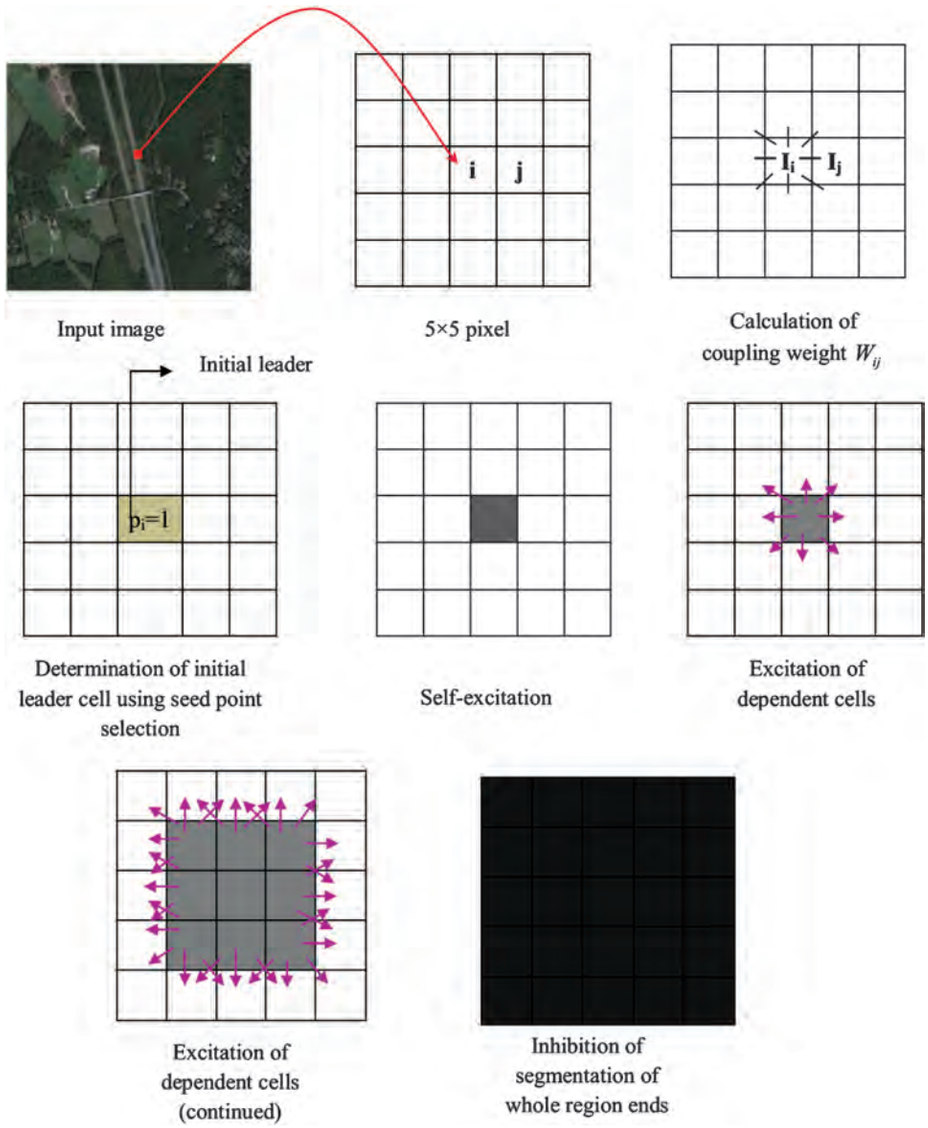

Fig. 6. Step by step process of proposed S-LEGION.

Stage 6: *Inhibition*. The process repeats these operations until no excitable cell is selected any more. If there is no excitable cell any more, the process performs "inhibition, region labeling" of stage 6, thereby completing the image segmentation of one region. The process repeats these operations until there is no no-excited leader cell any more, thereby completing the image segmentation of the image as a whole. In this processing of "inhibition," $x_i = 0$ and $z_i = 0$ are set for the cell i in the excitation state and if $p_i = 1$, $p_i = 0$ is set. The intermediate steps of S-LEGION are given in Figure 6 to better understand the concept clearly.

First, S-LEGION traces a road until a stopping criterion is met. Then, instead of terminating the process, the results are passed to the GHKF algorithm which tries to find the leader and continuation of the road after a possible obstacle or to identify all possible road branches that might exist on the other side of a road junction.

3.4. Phase II: Gaussian Hermit Kalman Filter

In this phase, a non-linear filter is employed to extract the remaining road from the satellite image. To initialize the GHKF phase, the S-LEGION phase relocates the information about its last successful step of the present road segment onto the GHKF phase. The GHKF[23] begins its work with a single road branch by using the last successful state estimate of the S-LEGION phase as its initial state y_1.

Prediction stage:

1. Find the root y_i, $i = 1, \ldots, p$, of the Hermite polynomial $H_p(y)$.

2. Compute the corresponding weights

$$w_i = \frac{2^{p-1}p!}{p^2[H_{p-1}(y_i)]^2}$$

3. Use the product rule to expand the points to a n dimensional lattice of p^n points ξ_i, $i = 1, \ldots, p^n$, with corresponding weights.
4. Propagate the cubature points. The matrix square root is the lower triangular cholesky factor.

$$Y_{i,q-1|q-1} = \sqrt{2P_{q-1|q-1}}\,\xi_i + m_{q-1|q-1}$$

5. Evaluate the cubature points with the dynamic model function

$$Y^*_{i,q|q-1} = f(Y_{i,q-1|q-1})$$

6. Estimate the predicted state mean

$$m_{q|q-1} = \sum_{i=1}^{p^n} w_i Y^*_{i,q|q-1}$$

7. Estimate the predicted error covariance

$$P_{q|q-1} = \sum_{i=1}^{p^n} w_i Y^*_{i,q|q-1} Y^T_{i,q|q-1} - m_{q|q-1}m^T_{q|q-1} + Q_{q-1}$$

Update stage:

1. Repeat steps 1–3 from earlier to get the p^n cubature points and their weights.
2. Propagate the cubature points.

$$X_{i,k|k-1} = \sqrt{2P_{k|k-1}\xi_i} + m_{k|k-1}$$

3. Evaluate the cubature points with the help of the measurement model function

$$Y_{i,k|k-1} = h(X_{i,k|k-1})$$

4. Estimate the predicted measurement

$$\hat{y}_{k|k-1} = \sum_{i=1}^{p^n} w_i Y_{i,k|k-1}$$

5. Estimate the innovation covariance matrix

$$S_{k|k-1} = \sum_{i=1}^{p^n} w_i Y_{i,k|k-1} Y^T_{i,k|k-1} - \hat{y}_{k|k-1}\hat{y}^T_{k|k-1} + R_k$$

6. Estimate the cross-covariance matrix

$$P_{xy,x|k-1} = \sum_{i=1}^{p^n} w_i X_{i,k-1|k-1} Y^T_{i,k|k-1} - m_{k|k-1}\hat{y}^T_{k|k-1}$$

7. Calculate the Kalman gain term and the smoothed state mean and covariance

$$K_k = P_{xy,k|k-1}S^{-1}_{k|k-1}$$

$$m_{k|k} = m_{k|k-1} + K_k(y_k - \hat{y}_{k|k-1})$$

$$P_{k|k} = P_{k|k-1} - K_k P_{yy,k|k-1}K^T_k$$

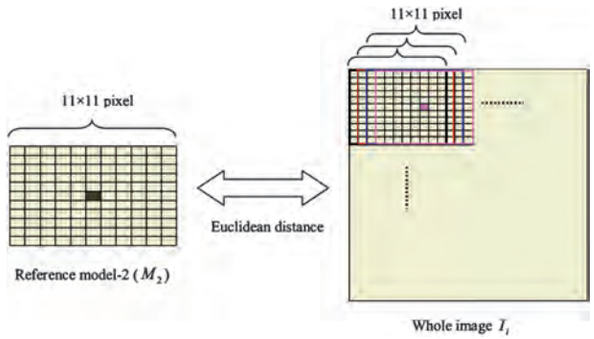

Fig. 7. Euclidean distance between reference model-2 and whole image.

3.5. Phase III: S-LEGION

In the final phase, if any road region cannot be extracted through first two phases, again phase-3 will continue the tracing process using S-LEGION. In this phase, the leader is selected through reference model-2 (M_2). The new leader selection is done by the following process:

- At first, Euclidean distance between reference model-2 (M_2) and whole image (I_i) are used to find the new leader pixel for road extraction. The Euclidean distance is calculated for every (11×11) pixel in the original image or (whole image). The new leader is selected as shown in Figure 7.

$$Ed_3 = \sum_{R_i,G_iB_i=1}^{N} \sqrt{\frac{(R_i^2 - RI_i) + (G_i^2 - GI_i) + (B_i^2 - BI_i)}{3}}$$

Where, $R_i^2 \rightarrow$ indicates ith pixel point of reference model-2 (for R component), $RI_i \rightarrow$ indicates ith pixel point of whole image I_i, $G_i^2 \rightarrow$ indicates ith pixel point of reference model-2 (for G component), $GI_i \rightarrow$ indicates ith pixel point of whole image I_i, $B_i^2 \rightarrow$ indicates ith pixel point of reference model-2 (for B component), $BI_i \rightarrow$ indicates ith pixel point of whole image I_i.

- From the above minimized pixel, the remaining and completing road extraction processes are performed.

4. SIMULATION RESULT AND DISCUSSION

This section presents the results obtained from the experimentation and its detailed discussion about the results. The proposed approach of road extraction technique is experimented with the satellite image dataset and the result is evaluated with the sensitivity, specificity and accuracy.

(a) **(b)** **(c)**

Fig. 8. Input satellite images.

RESEARCH ARTICLE

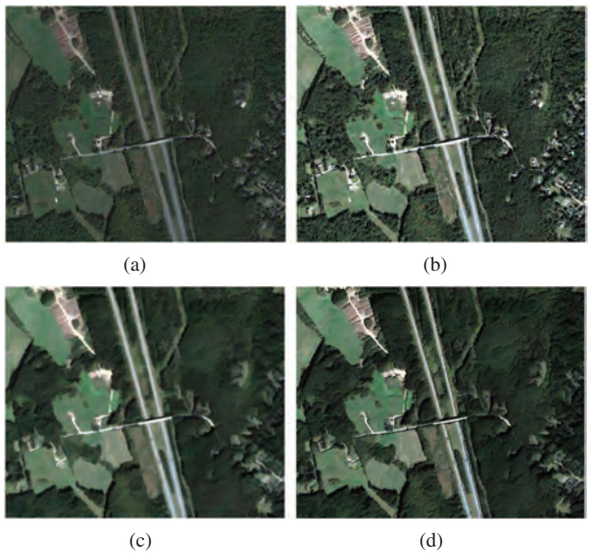

Fig. 9. (a) Input satellite image 1, (b) after contrast adjustment, (c) after applied morphological operation, (d) after applied Laplace filter.

4.1. Experimental Setup and Dataset Description

The proposed technique is performed in a windows machine having configurations Intel (R) Core i5 processor, 3.20 GHz, 4 GB RAM, and the operating system platform is Microsoft Wnidow 7 Professional. We have used mat lab latest version (7.12) for the proposed technique.

In this technique, we have used satellite road images and this satellite image collected through internet. The input image size is 1200 by 900 pixels. Figure 8 shows input road area satellite images.

Table II. Selected initial leader from the three input satellite images.

Satellite images	Seed point or pixel's location	Cluster 10	Cluster 15	Cluster 20
	ith row jth column pixel	$i = 378$ $j = 534$	$i = 372$ $j = 532$	$i = 390$ $j = 535$
	ith row jth column pixel	$i = 494$ $j = 375$	$i = 484$ $j = 370$	$i = 455$ $j = 364$
	ith row jth column pixel	$i = 335$ $j = 491$	$i = 335$ $j = 494$	$i = 334$ $j = 494$

Table III. Proposed tracking results against previous method for different clusters in image-1.

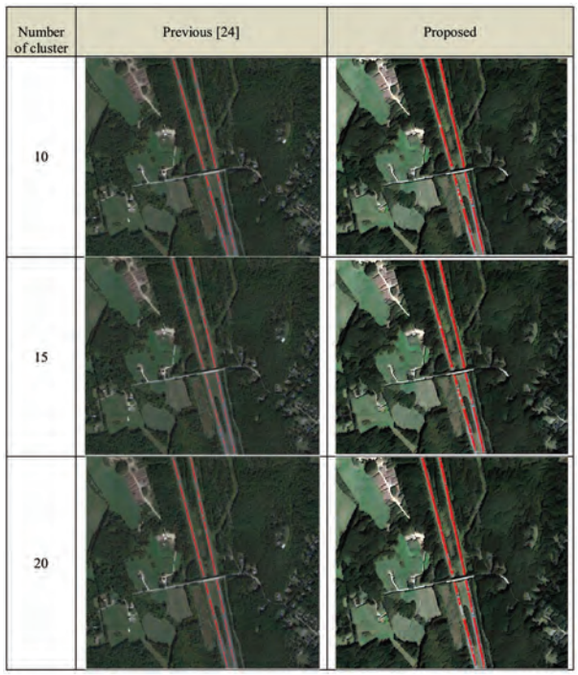

4.2. Evaluation Metrics

The results are evaluated using key evaluation matrices called sensitivity, specificity and accuracy.[25] The evaluation of proposed technique in different satellite

Table IV. Proposed tracking results against previous method for different clusters in image-2.

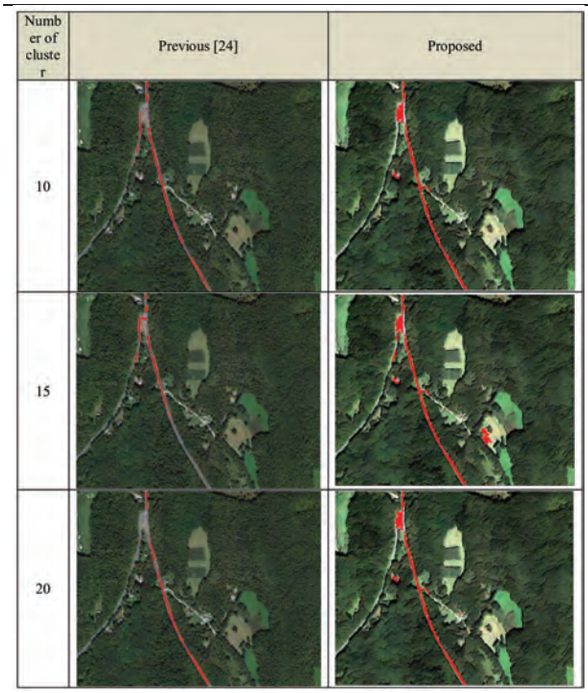

RESEARCH ARTICLE

Table V. Proposed tracking results against previous method for different clusters in image-3.

Number of cluster	Previous [24]	Proposed
10	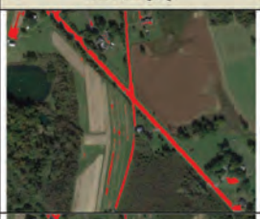	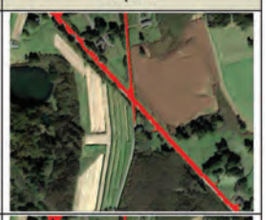
15		
20		

images are carried out using the following metrics as per equations:

$$\text{Sensitivity} = \frac{TP}{TP+FN}$$

$$\text{Specificity} = \frac{TN}{TN+FP}$$

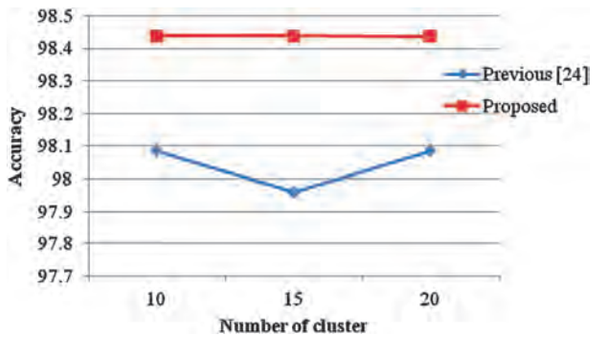

Fig. 10. Accuracy plot of proposed against existing[24] for image-1.

$$\text{Accuracy} = \frac{TN+TP}{TN+FP+FN+FP}$$

Where, TP stands for True Positive, TN stands for True Negative, FN stands for False Negative and FP stands for False Positive. *Sensitivity* is the proportion of true positives that are correctly identified by a proposed method. It shows how good the test is in detecting a road. *Specificity* is the proportion of the true negatives correctly identified by proposed method. It suggests how good the test is in identifying normal (negative) condition. *Accuracy* is the proportion of true results, either true positive or true negative, in a population.

4.3. EXPERIMENTAL RESULTS

4.3.1. Pre-Processing Steps

Figure 9(a) shows the input image. Figure 9(b) shows results of after contrast adjustment. Figure 9(c) shows the results of after applied morphological operation. 9(d) shows the results of after Laplace filter.

Table VI. Comparison table of proposed technique against existing technique.[24]

Satellite images	Number of cluster	Previous technique[24]				Proposed technique			
		Sensitivity	Specificity	Accuracy (%)	Time (sec)	Sensitivity	Specificity	Accuracy (%)	Time (sec)
	10	22.591	100	98.085	525	37.137	99.993	98.438	350
	15	17.438	100	97.960	600	37.137	99.993	98.438	450
	20	22.591	100	98.085	675	37.122	99.992	98.437	350
	10	24.336	100	98.452	100	29.973	99.869	98.487	75
	15	17.404	99.99	98.307	140	32.395	99.748	98.369	85
	20	21.942	100	98.403	300	29.678	99.851	98.414	225
	10	69.469	99.348	98.220	75	47.404	99.961	97.976	45
	15	45.388	99.930	97.871	140	46.880	99.947	97.943	115
	20	52.869	99.730	97.961	80	46.940	99.961	97.958	45

RESEARCH ARTICLE

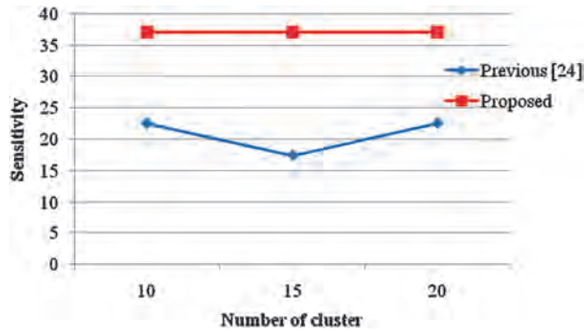

Fig. 11. Sensitivity plot of proposed against existing[24] for image-1.

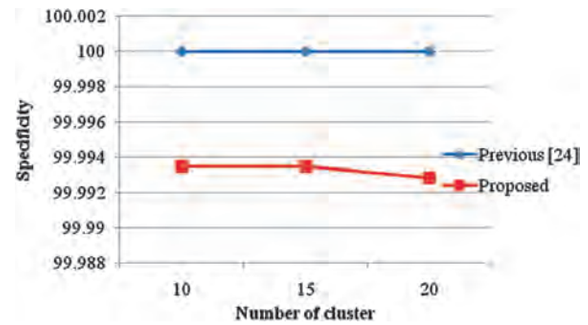

Fig. 12. Specificity plot of proposed against existing[24] for image-1.

4.3.2. Initial Leader Selection

In Table II, the algorithm starting from the initial point is tabulated. Here, the locations of the initial leader pixel for three images for three clusters are given.

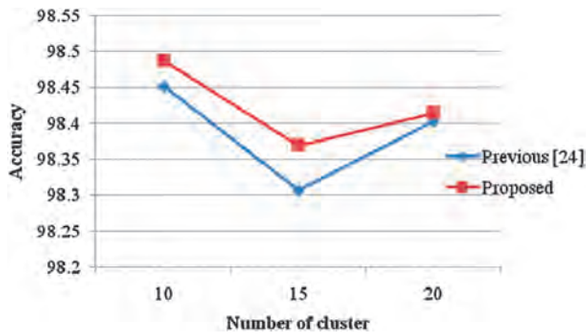

Fig. 13. Accuracy plot of proposed against existing[24] for image-2.

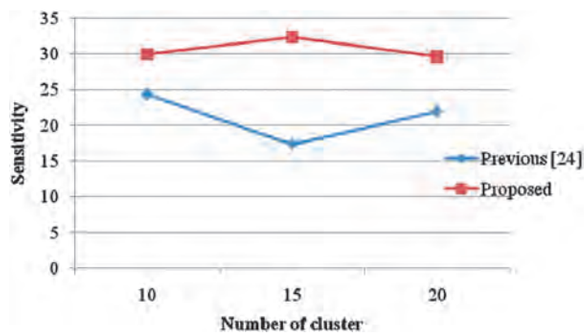

Fig. 14. Sensitivity plot of proposed against existing[24] for image-2.

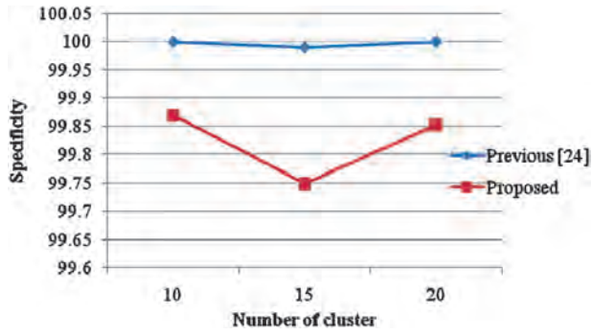

Fig. 15. Specificity plot of proposed against existing[24] for image-2.

4.3.3. Tracking Performance

To evaluate the performance of our proposed approach, we compare our results with our previous method.[24] We have chosen three images to show in detail behavior of the proposed approach. In the three images, a sinuous but very homogeneous road is shown. The output road sides appear in red. The road tracking performances of proposed and previous approaches with three images are presented in Tables III–V.

4.4. Comparative Analysis

To evaluate the performance of our proposed approach, we compare our results with our previous method.[24] Table VI shows the performance of the proposed approach.

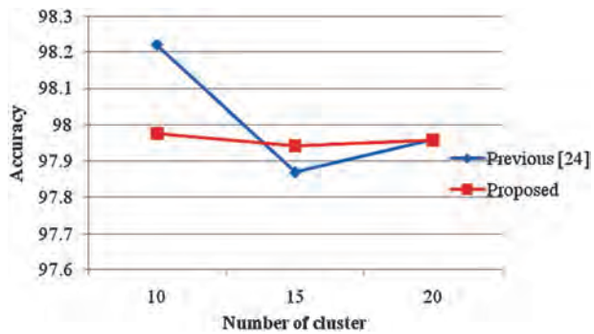

Fig. 16. Accuracy plot of proposed against existing[24] for image-3.

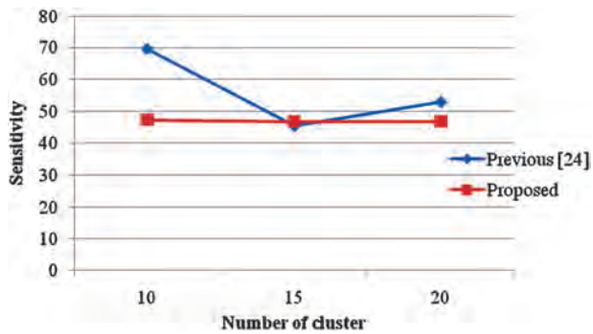

Fig. 17. Sensitivity plot of proposed against existing[24] for image-3.

RESEARCH ARTICLE

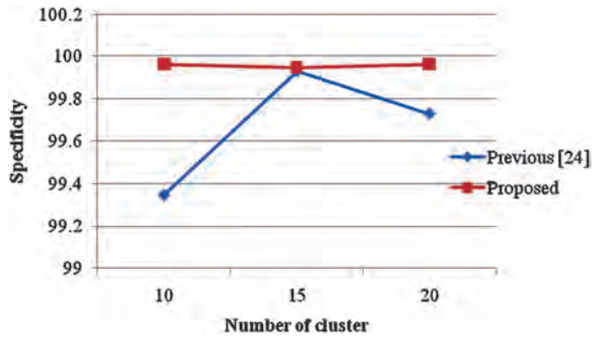

Fig. 18. Specificity plot of proposed against existing[24] for image-3.

For image 1, the performance graphs are plotted are furnished in Figures 10 to 12. In Figure 10, the proposed approach achieves an accuracy of about 98.438% whereas; our previous method is able to achieve only 98.085% for cluster 10. For image 2, the performance graphs are plotted and are furnished in Figures 13 to 15. In Figure 13, the proposed approach has achieved an accuracy of about 98.487% where, our previous method has achieved only 98.452% for cluster 10. For image 3, the performance graphs are plotted and are furnished in Figures 16 to 18. As shown in Figure 3, the previous approach achieves somewhat better results when compared to the proposed approach as far as accuracy is concerned, but our proposed technique ushers in better performance in terms of sensitivity and specificity when compared to the previous technique.[24] From the Table VI, it is seen that the proposed method shows a good performance in the road extraction from high resolution satellite images.

5. CONCLUSION

We have developed an efficient algorithm based on a unique combination of the S-LEGION and GHKF as a road-tracing approach for satellite images. This approach consists of three phases, such as phase I, phase II and phase III. In phase I, the S-LEGION is performed until the stopping criterion is met. Then, without terminating the process, the results are passed on to the phase I, where GHKF tries to trace the continuation of the road after a possible obstacle. Finally, if any road segment cannot be extracted through phase I and phase II, again S-LEGION is performed in phase III for the remaining road extraction. Our result indicates that, the proposed approach gives better results than several other methods in the literature. Furthermore, the proposed method can both get a faster detecting speed comparable to that of previous method and can more reliably detect the roads.

RESEARCH ARTICLE

References

1. A. P. D. Poz, R. A. B. Gallis, and João F. C. da Silva, *IEEE Geosciences and Remote Sensing Letters* 7 **(2010)**.
2. J. Hu, A. Razdan, J. C. Femiani, M. Cui, and P. Wonka, *IEEE Transactions on Geoscience and Remote Sensing* 45 **(2007)**.
3. Y. Shao, B. Guo, X. Hu, and L. Di, *IEEE Journal of Selected Topics in Applied Earth Observations and Remote Sensing* 4 **(2011)**.
4. C. He, Z.-X. Liao, F. Yang, X.-P. Deng, and M.-S. Liao, *IEEE Journal of Selected Topics in Applied Earth Observations and Remote Sensing* 5 **(2012)**.
5. A. P. D. Poz, R. A. B. Gallis, João F. C. da Silva, and Érico F. O. Martins, *IEEE Geosciences and Remote Sensing Letters* 9 **(2012)**.
6. Z. Miao, W. Shi, H. Zhang, and X. Wang, *IEEE Geoscience and Remote Sensing Letters* 10 **(2013)**.
7. S. Roessner, K. Segl, U. Heiden, and H. Kaufmann, *IEEE Trans. Geosci. Remote Sens.* 39, 1525 **(2001)**.
8. J. B. Mena, *Pattern Recognit. Lett.* 24, 3037 **(2003)**.
9. M. Kass, A. Witkin, and D. Terzopoulos, Snakes: Active contour models, *Proc. 1st Int. Conf. Comput. Vision*, London, U.K. **(1987)**, pp. 259–268.
10. T. Kim, S. R. Park, M. G. Kim, S. Jung, and K. O. Kim, *Photogramm. Eng. Remote Sens.* 70, 1417 **(2004)**.
11. J. Zhou, W. F. Bischof, and T. Caelli, *ISPRS J. Photogramm. Remote Sens.* 61, 108 **(2006)**.
12. X. Hu, C. V. Tao, and Y. Hu, *Int. Arch. Photogramm. Remote Sens. Spatial Inf. Sci.* 35, 320 **(2004)**.
13. A. Gruen and H. Li, *Photogramm. Eng. Remote Sens.* 63, 985 **(1997)**.
14. A. Baumgartner, C. Steger, H. Mayer, W. Eckstein, and H. Ebner, *Photogramm. Eng. Remote Sens.* 65, 777 **(1999)**.
15. A. Baumgartner, S. Hinz, and C. Wiedemann, *Int. Arch. Photogramm. Remote Sens. Spatial Inf. Sci.* 34, 28 **(2002)**.
16. S. Movaghati and A. Moghaddamjoo, *IEEE Transactions on Geoscience and Remote Sensing* 48 **(2010)**.
17. T. Peng, I. H. Jermyn, V. Prinet, Member, and J. Zerubia, *IEEE Journal of Selected Topics in Applied Earth Observations and Remote Sensing* 1 **(2008)**.
18. F. Dell'Acqua and P. Gamba, *IEEE Trans. Geosci. Remote Sens.* 39, 2287 **(2001)**.
19. M. J. Song and D. Civco, *Photogramm. Eng. Remote. Sens.* 70, 1365 **(2004)**.
20. W. Z. Shi and C. Q. Zhu, *IEEE Trans. Geosci. Remote Sens.* 40, 511 **(2002)**.
21. P. Gamba, F. Dell'Acqua, and G. Lisini, *IEEE Geosci. Remote Sens. Lett.* 3, 387 **(2006)**.
22. Rohit Maurya, Shalini Singh, P. R. Gupta, and Manish Kumar Sharma, *International Journal of Advanced Engineering Sciences and Technologies* 5, 290 **(2011)**.
23. G. Chalasani and S. Bhaumik, Bearing only tracking using gauss-hermite filter, *7th IEEE Conference on Industrial Electronics and Applications (ICIEA)* **(2012)**, pp. 1549–1554.
24. K. Madhan Kumar and R. Kanthavel, *International Review on Computers and Software (IRECOS)* 8 **(2013)**.
25. W. Zhu, N. Zeng, and N. Wang, Sensitivity, specificity, accuracy, associated confidence interval and roc analysis with practical SAS implementations, *Proceedings of the SAS Conference*, Baltimore, Maryland **(2010)**, p. 9.
26. J. Yuan, D. Wang, B. Wu, L. Yan, and R. Li, *IEEE Transactions on Geoscience and Remote Sensing* 49 **(2011)**.

Received: 3 February 2016. Accepted: 25 February 2016.